

AUGMENT LIKE THERE'S NO TOMORROW: CONSISTENTLY PERFORMING NEURAL NETWORKS FOR MEDICAL IMAGING

Joona Pohjonen^{1,†,*}, Carolin Stürenberg^{1,†}, Atte Föhr¹, Reija Randen-Brady³, Lassi Luomala^{1,3}, Jouni Lohi³, Esa Pitkänen^{2,4,5,‡}, Antti Rannikko^{1,5,6,‡}, and Tuomas Mirtti^{1,4,5,‡}

¹Research Program in Systems Oncology, Faculty of Medicine, University of Helsinki

²Institute for Molecular Medicine Finland (FIMM), HiLIFE, University of Helsinki

³Department of Pathology, Helsinki University Hospital

⁴Research Program in Applied Tumor Genomics, Faculty of Medicine, University of Helsinki

⁵iCAN Digital Precision Cancer Medicine Flagship, Finland

⁶Department of Urology, Helsinki University Hospital

[†]Authors contributed equally

[‡]Senior author

ABSTRACT

Deep neural networks have achieved impressive performance in a wide variety of medical imaging tasks. However, these models often fail on data not used during training, such as data originating from a different medical centre. How to recognise models suffering from this fragility, and how to design robust models are the main obstacles to clinical adoption. Here, we present general methods to identify causes for model generalisation failures and how to circumvent them. First, we use *distribution-shifted datasets* to show that models trained with current state-of-the-art methods are highly fragile to variability encountered in clinical practice and then develop a *strong augmentation* strategy to address this fragility. Distribution-shifted datasets allow us to discover this fragility, which can otherwise remain undetected after validation against multiple external datasets. Strong augmentation allows us to train robust models achieving consistent performance under shifts from the training data distribution. Importantly, we demonstrate that strong augmentation yields biomedical imaging models which retain high performance when applied to real-world clinical data. Our results pave the way for the development and evaluation of reliable and robust neural networks in clinical practice.

1 INTRODUCTION

Through digitalisation and neural network-based solutions, pathology is experiencing its third revolution [1]. Neural networks have been applied to tissue diagnostics with impressive results, often surpassing human counterparts in consistency, speed and accuracy [2, 3]. Despite promising results, many recent works have demonstrated neural networks performing substantially worse on datasets not used during training [4, 5, 6, 7, 8, 9, 10]. The two main challenges facing any neural network intended for clinical practice, stem from this generalisation problem [11]. How to train neural networks which perform consistently despite real-world variability, and how to demonstrate this consistency?

All clinical-grade neural networks should be robust to possible data distribution shifts encountered in a clinical practice [12].

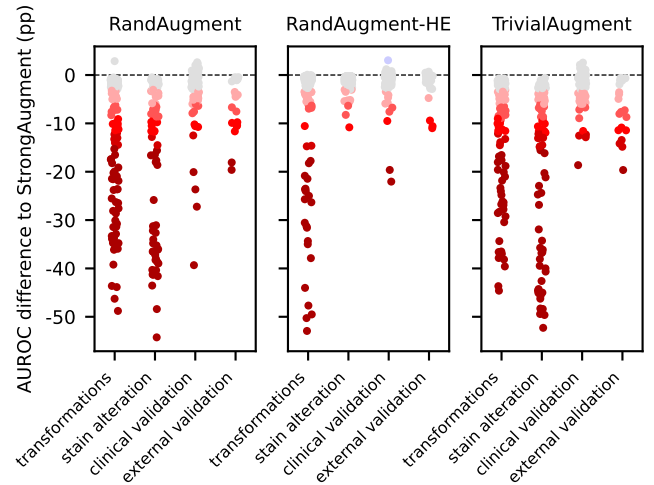


Figure 1: AUROC percentage-point (pp) difference between StrongAugment and the current state-of-the-art methods on a cancer classification task. Neural networks trained with strong augmentation retain similar performance on all distribution-shifted datasets, external datasets and clinical validation cases, achieving up to 50 percentage points higher discrimination performance than current state-of-the-art training methods.

This robustness is hard to assess and has been commonly evaluated by performance on external validation datasets. Although an important part of neural networks' path to clinic [11], external validation is limited to exposing a failure to generalise in the particular dataset, and cannot establish clinical usefulness, robustness or generalisation ability of a network [13]. Even when a neural network achieves good performance on multiple external datasets, it may fail on another dataset or a small subset of samples. Thus, there is a critical need for evaluating neural networks' robustness to data distribution shifts.

A promising solution for evaluating neural networks' robustness to distribution shifts is shifted evaluation [14]. With shifted evaluation, a distribution-shifting function is applied to every sample in a dataset to create a new distribution-shifted dataset. The used function completely describes any performance differences between the original and distribution-shifted datasets and thus provides a measure of robustness as well as guidance

*Correspondence: joona.pohjonen@helsinki.fi

Code: <https://github.com/jopo666/StrongAugment>

on how to improve the evaluated model in case of failure. For example, distribution-shifted datasets created with the JPEG-compression algorithm [15] can be used to measure whether a neural network is robust to artefacts created during image compression. Shifted evaluation has been used in several recent works, to demonstrate that neural networks are extremely fragile to even small distribution shifts from the training data distribution [12, 16, 17, 18].

Large multi-cohort datasets, which are representative of all types of data encountered in clinical practice, are often seen as the main solution to the generalisation problem [11]. Although important, larger datasets often have lower data quality [19] and different cohorts introduce their own biases, which makes training harder as neural networks overfit these biases easily [10, 12, 20]. Still, even a large high-quality multi-cohort dataset could not fully represent all types of data encountered in clinical practice, and other complementary methods for improving neural networks’ robustness are needed. Another popular method is stain normalisation, which reduces the variability (mainly colour) by normalising each image to a well-defined common standard [6, 21, 22, 23, 24, 25, 26]. Although stain normalisation can be useful, it is often computationally costly and does not fix the underlying problem of neural networks’ fragility towards distribution shifts [16].

Only a few solutions exist for increasing the robustness to distribution shifts from the training data. Recently proposed method of spectral decoupling [27] can be used to increase robustness to data distribution shifts, as well as avoid overfitting unwanted biases, for example in multi-cohort datasets [12]. Another solution is to introduce artificial variability to the images during neural network training, also known as augmentation. Augmentation has been shown to explicitly improve robustness to certain data distribution shifts [12, 25, 28]. For example, the sharpness of the scanned pathology slide images varies significantly between medical centres, scanning equipment and slide areas [12, 25]. By randomly adjusting the sharpness of the images during training, neural networks can be made robust to sharpness variations. Automatic augmentation strategies [29, 30, 31] have become a standard in training neural networks [32]. However, augmentation has been traditionally seen as a way to increase the amount of training data, and the development of augmentation strategies has not focused explicitly on improving neural networks’ robustness to data distribution shifts.

In this study, we propose general methods for evaluating and training robust neural networks intended for clinical practice. First, we demonstrate how shifted evaluation can be used to evaluate neural networks’ robustness to data distribution shifts, and thus also its generalisation ability in clinical practice. We discover that neural networks trained with the current state-of-the-art methods are extremely fragile to even small shifts from the training data distribution. We then develop an automatic augmentation strategy, StrongAugment, to address this fragility. Using large-scale heterogeneous histopathology data from several studies, we demonstrate that strong augmentation yields robust biomedical imaging models, while state-of-the-art methods achieve significantly lower discrimination performance (Figure 1).

2 MATERIALS AND METHODS

2.1 Shifted evaluation with distribution-shifted datasets

Let $x_1, \dots, x_n \in X$ denote a dataset with an unknown data generating process \mathcal{P} . To create a distribution shifted dataset $f(X)$, the distribution shifting function f is applied to each image $x_i \in X$, where $i \in 1, \dots, n$. Although the data generating process \mathcal{P} is unknown, any performance differences between the datasets $f(X)$ and X are guaranteed to be due to the distribution shift defined by f . For example, if a given model achieves an accuracy of 0.9 for dataset X and 0.5 for dataset $f_{\text{invert}}(X)$, where $f_{\text{invert}}(x_i) = 255 - x_i$, we can say that the given model is sensitive to the distribution shift caused by colour inversion.

The data generating process \mathcal{P} is inherently unknown for external datasets, as the image acquisition process cannot be exhaustively described. Thus, even when a given model passes external validation, it cannot establish clinical usefulness, robustness or generalisation ability of the model as there is no way of knowing why the model succeeds. External validation can only expose a failure to generalise, with no feedback given to the researcher on reasons for the failure.

2.1.1 Image transformations

To evaluate neural networks’ overall robustness to data distribution shifts, 15 image transformations are used to create distribution-shifted datasets. These datasets are denoted by $t(X, m)$, where t denotes the used transformation and m its magnitude. By increasing or decreasing magnitude m , the data distribution can be incrementally shifted further from the original distribution of dataset X . Figure 2 presents all selected transformations with examples of transformed images with different magnitudes.

The transformations and magnitudes, presented in Figure 2, were selected to create distribution-shifted datasets to evaluate neural networks’ overall robustness to data distribution shifts. It should be reasonable to expect a neural network to perform similarly on all of the images in Figure 2, and any potential failures will give important insights into the robustness of the model. Although some of the distribution-shifted datasets may not be directly encountered in routine clinical practice, they can still be useful in other ways. For example, if a given network performs consistently for dataset $\text{posterize}(X, 4)$, $\text{saturation}(X, 0)$ and $\text{jpeg}(X, 10)$, it could be possible to significantly reduce the size of large digital slides by reducing the number of bits, dropping colour channels or compressing images more heavily, without compromising model performance.

Noise, *emboss* and *jpeg* transformations are from the `augmentations` (1.2.1) library [33], *red*, *green*, *blue* transformations have been defined by us, and all other transformations are from the `torchvision` (1.11.1) library [34].

2.1.2 Haematoxylin and eosin stain intensities

Colours of the digital slide images can vary substantially due to differences in the staining processes and the choice of imaging equipment and its settings, especially between medical centres [25]. Although several transformations presented in Figure 2 evaluate robustness to changes in the colour of the images, none

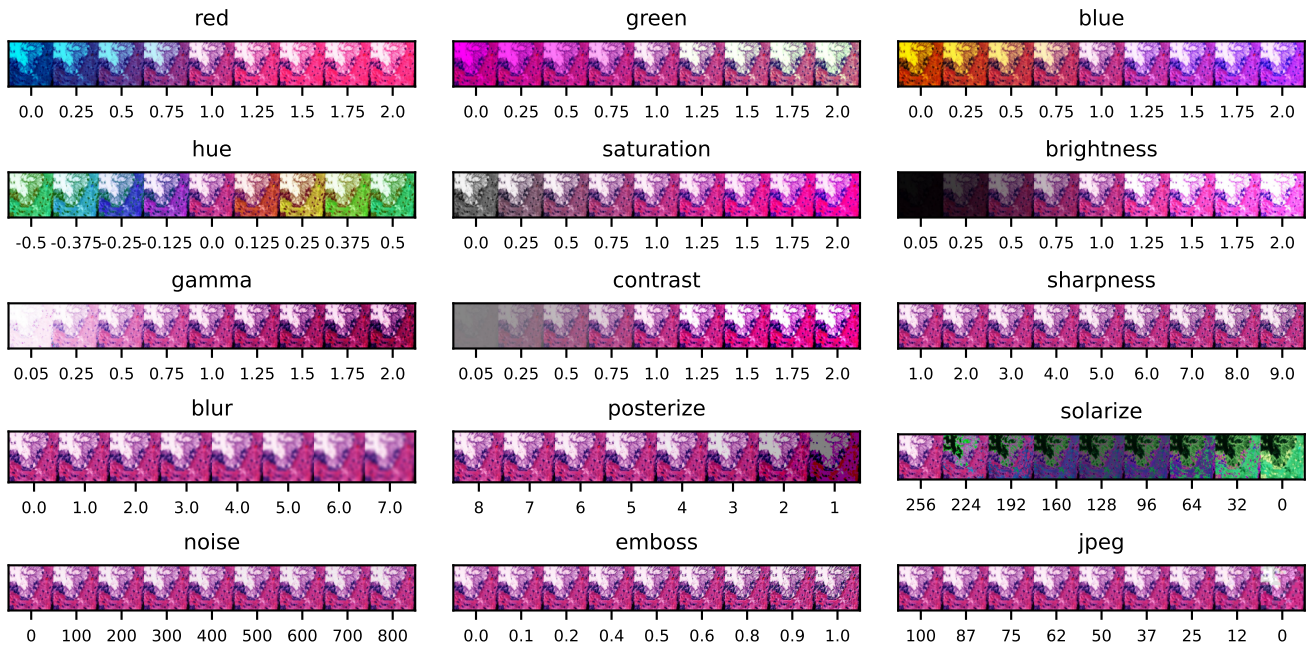


Figure 2: Examples of image transformations with $t(x_i, m)$, where transformation t is denoted by the figure title and magnitude m by the x-axis value.

of them explicitly measure robustness to data distribution shifts caused by differences in the staining process. For this reason, and to demonstrate the flexibility of distribution-shifted datasets, distribution-shifted datasets are created by adjusting the intensity of the haematoxylin and eosin stains.

To create a distribution-shifted dataset $stain(X, h, e)$, the Macenko method [21] is used to separate the haematoxylin and eosin stains, and then concentrations of each stain are multiplied with magnitudes h and e , respectively. For example, $h = 0.0, e = 1.0$ would remove the eosin stain completely from the image and $e = 1.0, m_h = 2.0$ would double the haematoxylin stain intensity. Figure 3 demonstrates example images from the distribution-shifted datasets. The mean stain vector of the original dataset is used to separate the stains.

2.2 StrongAugment

In this study, we create an automatic augmentation method, StrongAugment, which is designed to increase neural networks’ robustness to data distribution shifts from the training data. StrongAugment is compared to RandAugment [30], one of the most commonly used automatic augmentation methods, and TrivialAugment [31] which represents the current state-of-the-art in automatic augmentation. Importantly, implementations for both methods are easily accessible through the `torchvision` library, and thus likely used by other researchers in the field. Additionally, we compare StrongAugment to a HE-tailored variation of RandAugment, RandAugment-HE [35], which exploits prior knowledge of the presumable variation of histological images such as differences in the haematoxylin and eosin stains seen in Figure 3. This allows comparisons between augmentation strategies explicitly designed to increase robustness for certain data distribution shifts, such as HE-staining differences,

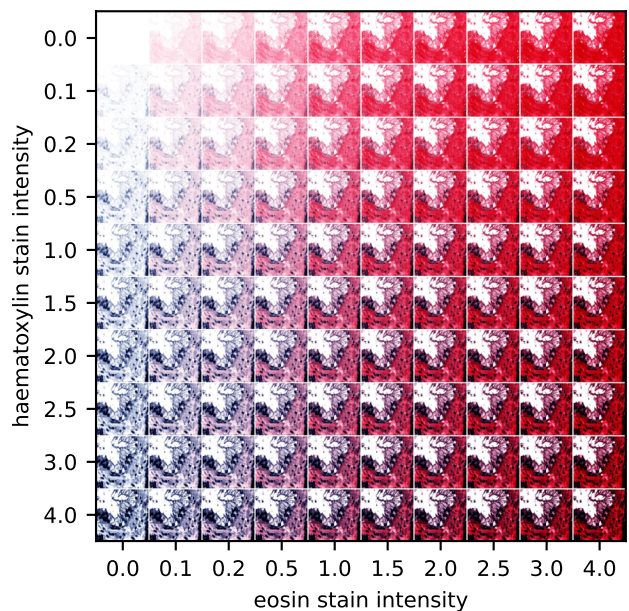


Figure 3: Examples of haematoxylin and eosin stain intensity adjustments where haematoxylin and eosin staining intensities are denoted by the y-axis and x-axis, respectively.

Table 1: Augmentation spaces of StrongAugment, RandAugment [30], RandAugment-HE [35] and TrivialAugment [31]. No effect column represents the magnitude which does not change the image where applicable. StrongAugment includes 6 additional transformations, Gaussian blurring and wider magnitude ranges for most of the common transformations. Examples for some of the transformations can be seen in Figure 2. Please note, that a hyper-parameter is used to further limit the magnitude ranges for RandAugment and RandAugment-HE.

Transformation	StrongAugment	RandAugment	RandAugment-HE	TrivialAugment	No effect
Identity	included	included	included	included	
Shear{X,Y}	[-145, 145]	[-17, 17]	[-51, 51]	[-145, 145]	1.0
Translate{X,Y}	[-32, 32]	[-72, 72]	[-30, 30]	[-32, 32]	0
Rotate	[-135, 135]	[-30, 30]	[-90, 90]	[-135, 135]	0
Saturation	[0.0, 2.0]	[0.1, 1.9]	[0.0, 5.5]	[0.01, 1.99]	1.0
Brightness	[0.1, 1.9]	[0.1, 1.9]	[0.0, 5.5]	[0.01, 1.99]	1.0
Contrast	[0.1, 1.9]	[0.1, 1.9]	[0.0, 5.5]	[0.01, 1.99]	1.0
Sharpness	[1.0, 2.0]	[0.1, 1.9]	[0.0, 5.5]	[0.01, 1.99]	1.0
Gaussian blur	[0.0, 2.0]	–	–	–	0.0
Solarize	[0, 255]	[0, 255]	–	[0, 255]	256
Posterize	[1, 8]	[4, 8]	–	[1, 8]	8
Equalize	included	included	included	included	
Auto contrast	included	included	included	included	
Grayscale	included	–	–	–	
Gamma	[0.1, 1.9]	–	–	–	1.0
Hue	[-0.5, 0.5]	–	–	–	0.0
Red	[0.01, 1.99]	–	–	–	1.0
Green	[0.01, 1.99]	–	–	–	1.0
Blue	[0.01, 1.99]	–	–	–	1.0
HED colour shift	–	–	[-0.9, 0.9]	–	0.0
HSV colour shift	–	–	[-0.9, 0.9]	–	0.0

HED: hematoxylin-eosin-DAB, HSV: and hue-saturation-value

and StrongAugment, which is designed to increase robustness for all distribution shifts.

StrongAugment applies a varying number of transformations sequentially to an image x . After x has been transformed two times, each consecutive transformation is applied with probability p , or until x has been transformed five times. Each transformation t and its magnitude m is sampled uniformly from an augmentation space A , which contains a specified list of transformations and a range of possible magnitudes for each transformation. After applying transformation t , the transformation t is removed from A . Only one affine transformation is allowed per image, to avoid cases where sequentially applied affine transformations move the image data out of the image. This allows significantly higher number of transformations than previous state-of-the-art augmentation methods [30, 31, 35, 36].

Table 1 represents the augmentation spaces of StrongAugment, RandAugment, RandAugment-HE and TrivialAugment, and Supplementary Figure S1 examples of augmented images with each method. StrongAugment has both a wider augmentation space A and a higher number of transformations applied per image. The augmentation space of StrongAugment contains all the same transformations as RandAugment and TrivialAugment, with six additional transformations. To enable stronger blurring of images, the default degenerate method implemented by the torchvision library was replaced with Gaussian blurring. No neural networks were trained while building the augmentation space to avoid overfitting the augmentation space to a

specific dataset. Transformations and their magnitude ranges were simply chosen to be as wide as possible.

RandAugment, TrivialAugment have been implemented by torchvision (1.11.1). RandAugment-HE has been implemented in a previous study [35]. For RandAugment, the magnitude m and number of operations n are set to $m = 10$ and $n = 2$ [32], and for RandAugment-HE to $m = 5$ and $n = 3$ [35]. For TrivialAugment there are no tunable hyper-parameters.

2.3 Training details

ResNet-RS50 [32] neural networks are used for all the experiments in this study. Dropout [37] and stochastic depth [38] are set to 0.2 [32] for all networks. For training, a random area of the image is cropped and resized to 160×160 pixels with either bi-linear, bi-cubic or nearest interpolation, and flipped horizontally and/or vertically with a probability of 0.5. Then the image is transformed with either StrongAugment, RandAugment, RandAugment-HE or TrivialAugment, a random area of the image is erased with an 0.2 probability, and either Mixup [39] or Cutmix [40] is applied for pair of images in a batch with an alpha value of 0.2. For testing, the images are resized to 224×224 pixels with bi-linear interpolation.

Adaptive sharpness aware minimisation [41] is used with $\rho = 0.05$ and Adam [42] with $\beta_1 = 0.9$, $\beta_2 = 0.999$ as the base optimiser. The learning rate is increased linearly from 10^{-6} to $0.0004 \times \text{batch_size}/256$ during the first 10 epochs and then reduced back to 10^{-6} with a cosine schedule. Label smoothing

is set to 0.1 [43]. All networks are trained for 150 epochs with a batch size of 1024. For each experiment, five neural networks are trained and the mean and standard deviation of the evaluation metric are reported.

Spectral decoupling [27] is used instead of weight decay, which has been shown to increase neural networks’ robustness for data distribution shifts [12]. Spectral decoupling coefficient is set to 0.0001 and weight decay to 0. For experiments, where spectral decoupling is intentionally left out to assess its effect on neural networks’ robustness, weight decay is set to 0.00004 [32].

PyTorch (1.10.0) ([44]) is used for training the neural networks, and ResNet-RS50, Mixup and Cutmix implementations are from the `timm` (0.5.4) library [45].

2.4 Evaluation metric

To evaluate the performance of a neural network in a given dataset, the area under the receiver operating characteristic curve (AUROC) is reported for each experiment. AUROC measures the ability to discriminate between positive and negative samples. The AUROC value corresponds to the proportion of positive and negative sample pairs, where the positive sample has a higher probability given by the classifier. AUROC values of 0.5 and 1.0 correspond to random and perfect discrimination, respectively.

2.5 Datasets

Seven different datasets from two tissue types, originating from four countries are used in this study. A basic summary of the datasets is presented in Table 2. All digital slide images are processed with the `HistoPrep` library (1.0.7) [50].

A total of 30 prostate cancer patients’ full glass slide sets from surgical specimens are annotated for classification into cancerous and benign tissue, where the cancerous areas were annotated in consensus by two observers (C.S., T.M.). All patients have undergone radical prostatectomy at the Helsinki University Hospital between 2014 and 2015. Each case contains 14 to 21 tissue section slides. Tissue sections have a thickness of 4 μm and were stained with haematoxylin and eosin in a clinical-grade laboratory at the Helsinki University Hospital Diagnostic Center, Department of Pathology. Two different scanners are used to obtain images of the tissue section slides at 20x magnification. Larger macro slides (whole-mount, 2x3 inch slides) are scanned with an Axio Scan Z.1 scanner (Zeiss, Oberkochen, Germany), and the normal size slides with a Panoramic Flash III 250 scanner (3DHistech, Budapest, Hungary). From the 30 patient cases, seven are set aside for a validation set. Digital slide images are cut into tiles with 1024×1024 pixels and 20% overlap, resulting in 4.7 million tiles with 10% containing cancerous tissue. For training, we selected all cancerous tiles and sample randomly the same amount of benign tiles to have equal amounts of positive and negative samples. We denote this dataset as Helsinki30.

Another set of 60 radical prostatectomy slides is also annotated into cancerous and benign tissue by one of six experienced pathologists as part of routine clinical diagnostics. All patients have undergone radical prostatectomy at the Helsinki University Hospital between 2019 and 2020. Each case contains 10 to 21 normal and macro tissue section slides of the prostate. Tissue sections have a thickness of 4 μm and are also stained with

haematoxylin and eosin in a clinical-grade laboratory at the Helsinki University Hospital Diagnostic Center, Department of Pathology. All slides are scanned with an Axio Scan Z.1 scanner. From the 60 patient cases, seven are set aside for a validation set. Digital slide images are cut into 1024×1024 pixel tiles with 20% overlap, resulting in 13.1 million tiles with 16% containing cancerous tissue. For training, we selected all cancerous tiles and sample randomly the same amount of benign tiles to have equal amounts of positive and negative samples. We denote this dataset as Helsinki60.

As external datasets, four publicly available prostate cancer datasets are used. These datasets yield five external datasets from three different countries.

The PANDA development dataset contains 10616 prostate biopsy slides from 2113 patients from Radboud University Medical Center between 2012 and 2017 and Karolinska Institutet (Stockholm, Sweden) between 2012 and 2014 [46]. The digital slide images are cut into 512×512 pixel tiles with 20% overlap resulting in 609180 (48% cancer) and 780694 (23% cancer) tiles from Radboud University Medical Center and Karolinska Institutet, respectively. Tile images were labelled as cancerous if there was any overlap with the cancerous annotations. Validation splits are omitted for both datasets as patient identifiers are missing from the publicly available data. We denote the datasets from Radboud University Medical Center and Karolinska Institutet as Radboud and Karolinska, respectively.

The PESO dataset contains tissue section slides from patients who have undergone a radical prostatectomy at the Radboud University Medical Center (Nijmegen, the Netherlands) between 2006 and 2011 ([47, 48]). The dataset contains images with 2500×2500 pixels annotated by a uropathologist as either cancerous or benign. These images are cut into 512×512 pixel tiles with 20% overlap, resulting in 5655 tiles with 45% containing cancerous tissue.

The Gleason2019 dataset contains 333 prostate tissue microarray spots from 231 patients who had undergone radical prostatectomy at Vancouver General Hospital between 1997 and 2011 [49]. These digital slide images are cut into 224×224 pixel tiles with 20% overlap resulting in 94230 tiles with 88.5% containing cancerous tissue.

To evaluate augmentation strategies on training data from a different tissue type, a dataset was compiled from 167 patients with renal cell carcinoma (clear cell). All patients had undergone radical nephrectomy at the Helsinki University Hospital between 2006 and 2013. Tissue sections were stained with haematoxylin and eosin in a clinical-grade laboratory at the Helsinki University Hospital Diagnostic Center, Department of Pathology. A total of 698 cancerous and 172 benign tissue microarray spots were gathered from the sections and scanned with Panoramic Flash III 250 scanner (3DHistech, Budapest, Hungary). Of the 167 patients, 24 were set aside for a validation set. Scanned tissue microarray spots were cut into tiles with 384×384 pixels and 20% overlap, resulting in 2.0 million tiles with 21% containing cancerous tissue. We denote this dataset as HelsinkiRCC.

2.5.1 Label noise

Each dataset used in this study has a variable annotation strategy as they stem from different projects. Thus, each dataset contains

Table 2: Datasets used in this study.

Name	Medical centre	Years	Images	Label noise	Reference
Helsinki30	Helsinki University Hospital	2014-2015	4.7 mil.	0.03%	[12]
Helsinki60	Helsinki University Hospital	2019-2020	13.1 mil.	17.0%	–
Karolinska	Karolinska Institutet	2012-2014	0.6 mil.	9.6%	[46]
Radboud	Radboud University Medical Center	2012-2017	0.8 mil.	3.9%	[46]
PESO	Radboud University Medical Center	2006-2011	5655	–	[47, 48]
Gleason2019	Vancouver General Hospital	1997-2011	94230	14.7%	[49]
HelsinkiRCC	Helsinki University Hospital	2006-2013	2.0 mil.	8.1%	–

different amounts of label noise. For this reason, the reported performances on different datasets are not directly comparable. For example, a perfect classifier would achieve 100% accuracy on a clean dataset, but only 80% accuracy on a dataset with 20% label noise. In reality, there are no perfect classifiers [51] and the decreased performance on an external dataset may also be caused by the fact that the classifier cannot generalise to the dataset. For this reason, the amount of label noise in a dataset should be estimated.

To estimate the amount of label noise in a given dataset, a neural network is trained on the dataset, and the training discrimination performance is reported. Due to overfitting, the estimate of label noise in the dataset can easily be deflated. To minimise overfitting, we use strong regularisation outlined in Section 2.3 with StrongAugment. To evaluate the accuracy of this estimation method, label noise is introduced to the Helsinki30 dataset, which contains the least amount of label noise based on a niche expert evaluation (T.M.). After flipping 0, 5, 10 and 20% of the labels in the Helsinki30 dataset, the estimated label noise is 0.03, 5.5, 10.21 and 20.16%, respectively.

The estimated amount of label noise in the Helsinki30, Helsinki60, Karolinska, Radboud, Gleason2019 and HelsinkiRCC datasets are 0.03%, 17.0%, 9.6%, 3.9%, 14.7% and 8.1%, respectively.

2.6 Clinical Validation

To evaluate neural networks’ robustness to distribution shifts encountered in routine clinical practice, several clinical validation cases were collected. Three surgical specimen paraffin blocks from patients who have undergone radical prostatectomy at the Helsinki University Hospital (HUS) in June of 2022, were collected. For each specimen, 36 serial tissue sections were stained in one of four HUS Diagnostic Centre’s clinical-grade laboratories, using one of three slide types. Each slide is then scanned with two different scanners at 20x magnification. The four medical centres are Hyvinkää Hospital (Hyvinkää, Finland), Jorvi Hospital (Espoo, Finland), Kotka hospital (Kotka, Finland) and Meilahti Hospital (Helsinki, Finland). The three microscope slides are Superfrost Plus (SP) (Fisher Scientific, Waltham, MA, United States), TOMO (Matsunami Glass, Bellingham, WA, United States) and Klinipath (KP) (VWR International, Radnor, PA, United States). The two scanners are Pannoramic 1000 (3DHitech, Budapest, Hungary) and Aperio AT2 (Leica Microsystems, Wetzlar, Germany). This produces 72 scanned slide images, which are annotated for classification into cancerous and benign tissue, by one observer (T.M.). There is consider-

able variability between medical laboratories, slide glasses and scanners, which is demonstrated in Supplementary Figure S2.

3 RESULTS

3.1 Robustness to data distribution shifts

First, neural networks’ robustness to data distribution shifts is evaluated with distribution-shifted datasets created from the PESO dataset. For each experiment, five neural networks are trained on the Helsinki30 dataset with either StrongAugment, RandAugment, RandAugment-HE or TrivialAugment while keeping all other hyper-parameters fixed.

First, the general robustness to data distribution shifts is evaluated using the distribution-shifted datasets, described in Section 2.1.1, with examples presented in Figure 2. Discrimination performances of the trained neural networks on these datasets are presented in Figure 4. Although all methods achieve similar performance on the original dataset, neural networks trained with either RandAugment, RandAugment-HE or TrivialAugment are highly sensitive to even small data distribution shifts, which is evident from the large performance differences between the original and distribution-shifted datasets. Neural networks trained with StrongAugment retain similar or significantly higher discrimination performances for all distribution-shifted datasets, even in cases where networks trained with other methods have degraded to no better than random discrimination. Notably, neural networks trained with StrongAugment are robust to distribution shifts not included in the augmentation space, such as Noise, Emboss and JPEG transformations. Comparably, neural networks trained with either RandAugment, RandAugment-HE or TrivialAugment are sensitive to many of the transformations included in their augmentation space, such as Hue and Brightness transformations.

Second, neural networks’ robustness to data distribution shifts caused by differences in the haematoxylin and eosin stain intensities is evaluated using the distribution-shifted datasets described in Section 2.1.2, with example images presented in Figure 3. Discrimination performances of the trained neural networks on these datasets are presented in Figure 5. Neural networks trained with either RandAugment, or TrivialAugment are highly sensitive to distribution shifts caused by changes in the haematoxylin and eosin stain intensities, and the discrimination performance degrades to no better than random with even small distribution shifts. Neural networks trained with StrongAugment retain their discrimination performance on all distribution-shifted datasets, even with datasets where networks

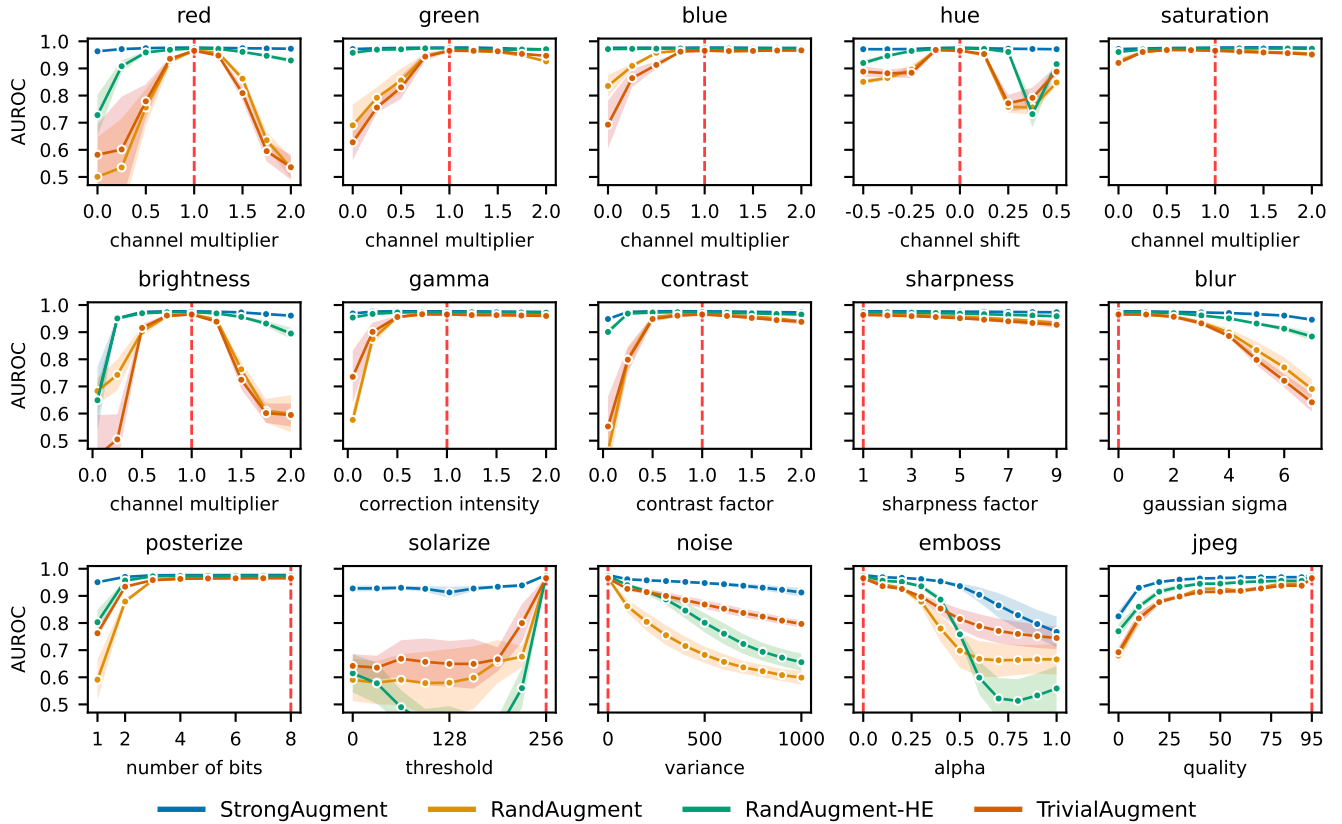


Figure 4: Robustness of neural networks, trained on the Helsinki30 dataset with either StrongAugment, RandAugment, RandAugment-HE or TrivialAugment, to distribution shifts caused by image transformations. The lines show the mean AUROC values and shaded regions with one standard deviation around the mean for the five trained networks. The distribution-shifted datasets $t(X_{\text{PESO}}, m)$ are represented by dots, where the title denotes the transformation t and the x-axis the magnitude m . Networks trained with StrongAugment retain their discrimination performance despite increasingly large distribution shifts, whereas the performance of networks trained with RandAugment or TrivialAugment degrade quickly with even small distribution shifts. This fragility is not discoverable by simply looking at the performance on the unmodified PESO dataset, denoted by dotted red lines.

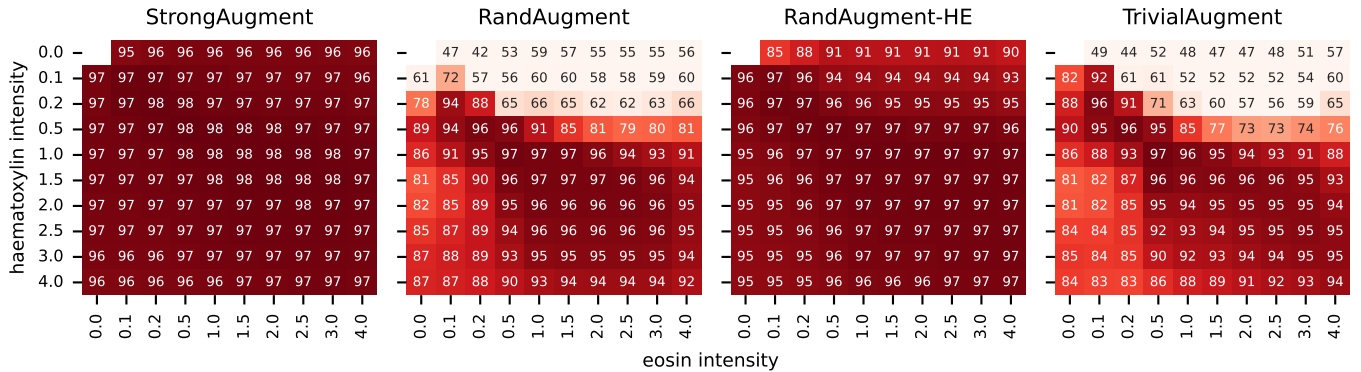


Figure 5: Robustness of neural networks, trained on the Helsinki30 dataset with either StrongAugment, RandAugment, RandAugment-HE or TrivialAugment, to distribution shifts caused by differences in the haematoxylin and eosin stain intensities. Each cell represents a given distribution-shifted dataset $\text{stain}(X_{\text{PESO}}, h, e)$, where h and e denote the magnitudes for haematoxylin and eosin stains, respectively. Cells are annotated with mean AUROC $\times 100$ value across the five trained networks, rounded to the closest integer. Neural networks trained with StrongAugment retain performance on all datasets, even when networks trained with RandAugment or TrivialAugment have degraded to no better than random discrimination. StrongAugment also outperforms RandAugment-HE, even though the latter method explicitly controls for staining differences.

trained with RandAugment or TrivialAugment have no better than random discrimination. StrongAugment also significantly outperforms RandAugment-HE, which explicitly controls for the distribution shifts caused by haematoxylin and eosin differences [35].

We recommend comparing the discrimination performances in Figures 4 and 5 to the example images in Figures 2, 3, respectively.

3.2 External validation

To assess, whether better performance on the distribution-shifted datasets translates to better performance on real-world datasets, we evaluate the trained neural networks on the Helsinki30, Helsinki60, Karolinska, Radboud [46], PESO [47] and Gleason2019 [49] datasets. To demonstrate that StrongAugment has not just been over-fitted to the Helsinki30 dataset used in Section 3.1, we also train and evaluate neural networks on the Helsinki60, Karolinska and Radboud datasets. For each experiment, five neural networks are trained with either StrongAugment, RandAugment, RandAugment-HE or TrivialAugment while keeping all other hyper-parameters fixed.

The discrimination performances of neural networks trained with StrongAugment, RandAugment, RandAugment-HE or TrivialAugment are presented in Figure 6. Compared to the current state-of-the-art methods, neural networks trained with StrongAugment achieve better or similar results on every external validation dataset. Networks trained with RandAugment, RandAugment-HE or TrivialAugment fail to generalise to several of the external datasets, despite the fact that the same networks achieve good results on other external validation datasets. For example, networks trained on the Helsinki30 dataset (first columns) with RandAugment or RandAugment-HE perform comparably to StrongAugment on the Helsinki60, Karolinska, Radboud and PESO datasets, but then achieve unacceptably low discrimination performances of 0.6 to 0.7 on the Gleason2019 dataset. Here, shifted evaluation allowed us to easily detect fragility to distribution shifts, which otherwise would have been missed if Gleason2019 dataset was not available.

As expected, neural networks trained on the datasets with more label noise achieve noticeably worse performance with all augmentation methods, including StrongAugment. Nevertheless, networks trained with StrongAugment still maintain an acceptable performance on all evaluation datasets, whereas the other methods result in no better than random discrimination performance. This is most apparent with the Karolinska (third columns) and Radboud (last columns) training datasets, where StrongAugment improves the mean discrimination performance over RandAugment and TrivialAugment by 0.116 to 0.196 on the Helsinki30 dataset, and by 0.099 and 0.181 on the Helsinki60 dataset.

In addition to improved performance, there is a significantly lower variance in the discrimination performances across the five trained networks when using StrongAugment. When training neural networks with StrongAugment, RandAugment, RandAugment-HE and TrivialAugment, the maximum difference between the best and worst-performing networks is 0.032, 0.132, 0.086 and 0.121, respectively.

3.3 Clinical validation

To assess neural networks’ robustness to actual data distribution shifts encountered in clinical practice, we evaluate five neural networks trained on the Helsinki30 dataset with clinical validation cases described in Section 2.6.

The discrimination performances for each of the 72 clinical validation cases are presented in Figure 7. Neural networks trained with StrongAugment generalise to all clinical validation cases, whereas each of the compared methods fails to generalise to several cases. StrongAugment achieves at least 0.03 better AUROC values in 24, 10, and 28 cases when compared to RandAugment, RandAugment-HE and TrivialAugment, respectively. StrongAugment achieves at least 0.03 worse AUROC value in only a single case. Without StrongAugment, neural networks fail to generalise to actual data distribution shifts encountered in clinical practice.

3.4 Effect of spectral decoupling

As spectral decoupling has been shown to increase robustness to data distribution shifts [12], we evaluate the effect spectral decoupling has on neural network performance. Five neural networks are trained on the Helsinki30 dataset, using either StrongAugment, RandAugment or TrivialAugment, and weight decay instead of spectral decoupling. The neural networks are then evaluated on the distribution-shifted datasets, adjusting haematoxylin and eosin stain intensities, described in Section 2.1.2.

The discrimination performances of the trained neural networks are presented in Supplementary Figure S3. Networks trained with StrongAugment achieve consistent results even without spectral decoupling, although there is a slight decrease in performance of up to four percentage points. Spectral decoupling is much more crucial for RandAugment and TrivialAugment, where the use of weight decay decreases the AUROC values by up to 25 percentage points. Based on these results, spectral decoupling is complementary with StrongAugment and crucial for training robust neural networks.

3.5 Other tissues

To assess whether the previous results are somehow specific to prostate tissue, five neural networks are trained with StrongAugment, RandAugment or TrivialAugment on the HelsinkiRCC dataset training split containing kidney tissue. The neural networks are then evaluated on distribution-shifted datasets created from the HelsinkiRCC validation split by adjusting haematoxylin and eosin stains similarly to Section 2.1.2.

The discrimination performances of the trained neural networks are presented in Supplementary Figure S4. Neural networks trained with StrongAugment achieve consistent performance on the distribution-shifted datasets, whereas the performance of networks trained with RandAugment and TrivialAugment degrades quickly with even small distribution shifts. These results indicate that neural network fragility is not specific to prostate tissue, and strong augmentation is helpful with other types of tissues as well. Additionally, it is demonstrated here that shifted evaluation can also be useful when extending the validation split, and not only external datasets.

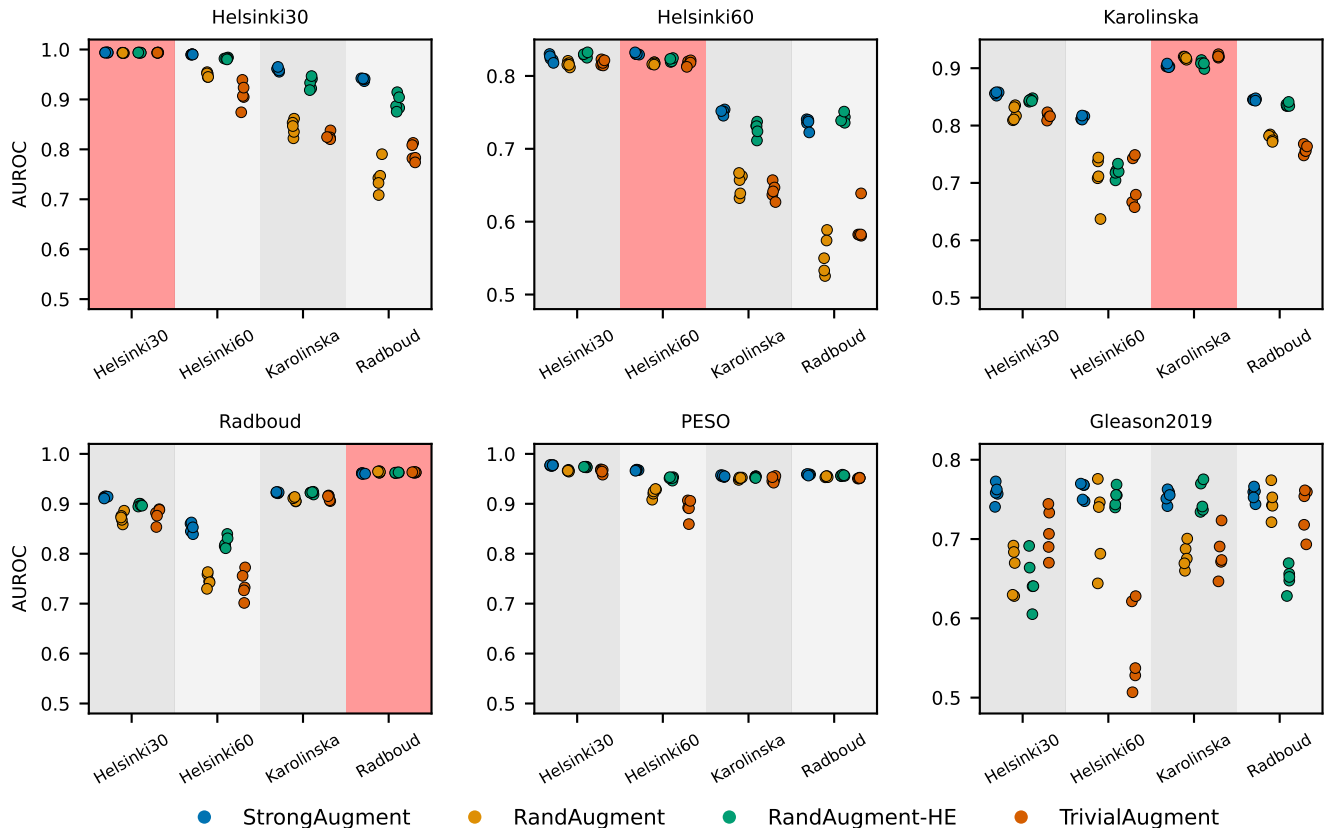


Figure 6: Discrimination performances of neural networks trained with StrongAugment, RandAugment, RandAugment-HE or TrivialAugment on four different training datasets. Each network is evaluated with five external datasets and the training dataset, denoted by a red box. Evaluation datasets are denoted by the figure titles and training datasets by the x-axis labels. Neural networks trained with StrongAugment achieve better or comparable performance on every evaluation dataset, whereas RandAugment, RandAugment-HE and TrivialAugment demonstrate a significant lack of generalisation ability with several evaluation datasets. Please note that the y-axes of Helsinki60, Karolinska and Gleason2019 evaluation datasets have been truncated to account for the label noise in these datasets.

4 DISCUSSION

Robustness evaluation is crucial for understanding the clinical usefulness, safety and accuracy of machine learning models intended for clinical practice [11]. Despite showing strong performance on multiple external validation datasets, state-of-the-art neural networks fail to generalise to multiple clinical validation cases. With shifted evaluation, this fragility can be discovered by simply extending the validation split with distribution-shifted datasets, and addressed with strong augmentation.

Although external validations will be a crucial part of any neural network’s path to clinic [11], there are serious limitations [13]. As the data-generating process is unknown, there is no way of knowing why the evaluated network fails or succeeds in external evaluation. By extending the external dataset with distribution-shifted datasets, it is possible to have known data generation functions, which completely describe any performance differences between the datasets. Thus, it is possible to discover cases where the network fails, and demonstrate robustness for the selected distribution shifts.

We believe that due to the lack of adequate evaluation methods, the role of augmentation as a method of increasing neural net-

works’ robustness to data distribution shifts has been largely unexplored. In medical imaging, some work has been done with training stain-invariant neural networks through augmentation [28, 35]. A comparison of different stain augmentation and normalisation methods concluded that augmentation is crucial for achieving good performance, but found slightly better results with light rather than strong augmentation [25]. As the results were based on external validation performance and augmentation was coupled with stain normalisation, it is likely that the fragility of neural networks was simply not discovered. With natural images, the development of augmentation methods has mostly focused on improving performance on the validation split of the ImageNet [52] dataset [29, 30, 31, 36]. Thus, light augmentation has been preferred over strong, which can reduce performance on in-distribution datasets, although the reduction in performance is often dwarfed when compared to the performance decreases on external datasets [19].

Interestingly, even though the augmentation space of RandAugment, RandAugment-HE or TrivialAugment contains a given transformation, this does not guarantee that the trained network becomes robust for the distribution shift caused by the transformation. For example, the *solarize* transformation is included in

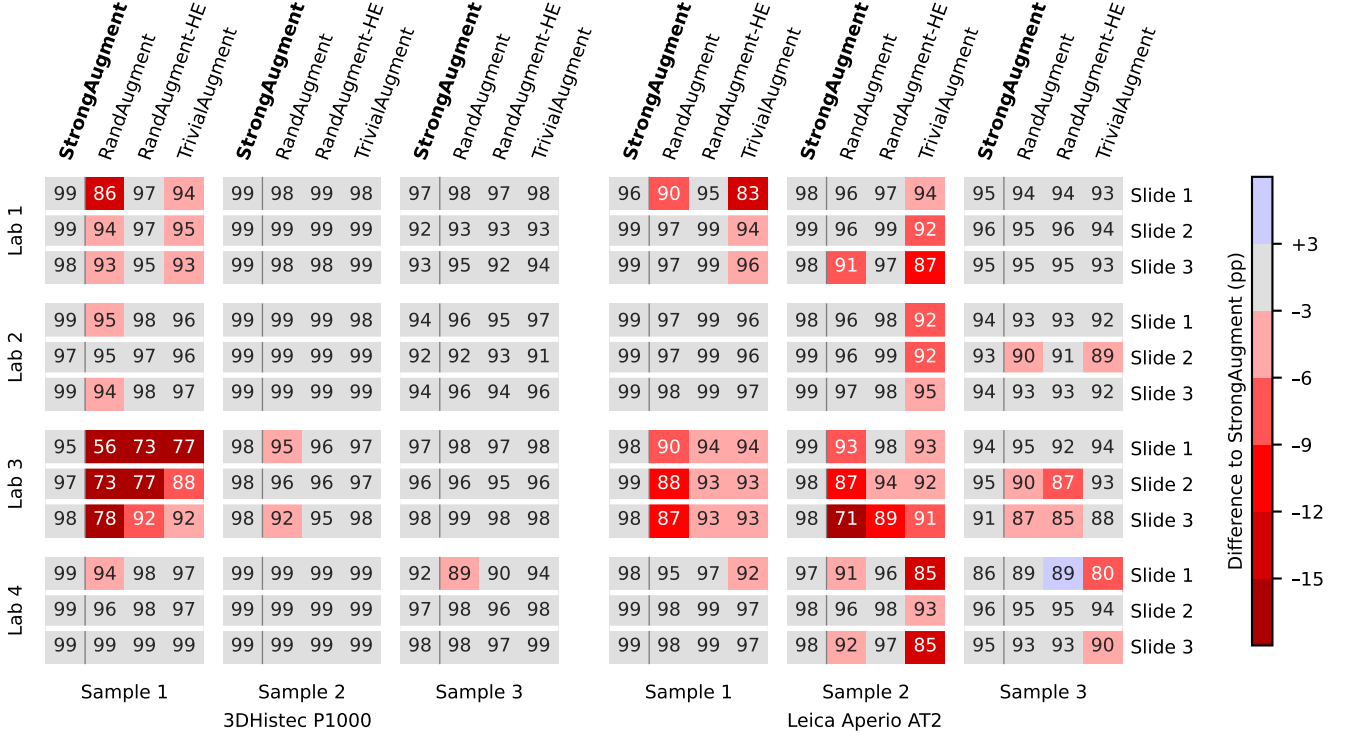


Figure 7: Discrimination performances of neural networks trained with StrongAugment, RandAugment, RandAugment-HE or TrivialAugment on 72 clinical validation cases. Each case is represented by a 1×4 block of cells, and due to different amounts of label noise, comparisons are valid only within each block. Each cell is annotated by AUROC $\times 100$ value and coloured based on the percentage point (pp) difference to StrongAugment. Neural networks trained with StrongAugment perform consistently on all clinical validation cases, whereas each of the compared methods fails to generalise to several clinical validation cases.

the augmentation spaces of RandAugment and TrivialAugment, but networks trained with either method are still extremely fragile for this distribution shift. TrivialAugment even has a wider augmentation space for the *brightness* transformation, but StrongAugment achieves 0.461 better AUROC when doubling the brightness of the images in the dataset. We speculate that the combination of a wider augmentation space, coupled with a significantly higher number of transformations per image makes neural networks trained with StrongAugment robust to distribution shifts included in its augmentation space. Additionally, the results of this paper suggest that networks trained with StrongAugment are also robust to other data distribution shifts, not just the ones included in the augmentation space.

Neural networks trained with StrongAugment achieve consistent results with distribution-shifted datasets, external validation and clinical validation cases. This is not the case for current state-of-the-art methods, which are extremely fragile to distribution shifts and fail to generalise to several external datasets and clinical validation cases. The performance decreases for networks trained with RandAugment, RandAugment-HE and TrivialAugment are unacceptable with most of the datasets, especially when considering that the decrease does not occur with networks trained with StrongAugment. The magnitude of differences we show between StrongAugment and current state-of-the-art methods are rarely reported. For example, TrivialAugment is reported to increase AUROC by 0.005 over RandAugment, and RandAugment-HE [35] to increase the AUROC by 0.006

over the compared method [25]. In comparison, StrongAugment increases AUROC by at least 0.1 in 104, 29 and 102 datasets for RandAugment, RandAugment-HE and TrivialAugment, respectively.

Although neural networks trained with StrongAugment achieve unprecedented results, it does not solve the generalisation problem in medical imaging on its own. Other methods which increase neural networks’ robustness to data distribution shifts should be used. For example, spectral decoupling has been shown to increase robustness to data distribution shifts [12], and it is highly complementary with StrongAugment (Figure S3). Also, high-quality and representative datasets are crucial for training neural networks intended for clinical practice. This is demonstrated in Figure 6, where datasets with more label noise achieve lower discrimination performance on external validation. With StrongAugment this gap is significantly smaller, emphasising the usefulness of strong augmentation on lower-quality datasets. With StrongAugment, the collection of representative training datasets can now focus on biological representativeness, instead of using multiple different scanners or staining pipelines.

5 CONCLUSIONS

In this study, we have exposed the fragility of neural networks using shifted evaluation. Shifted evaluation can be used to thoroughly evaluate a neural network while providing a measure

of robustness to distribution shifts, and guidance on how to improve the network in case of failure. To address the exposed fragility of neural networks, we developed an augmentation strategy which allows neural networks to be robust to data distribution shifts from the training data. StrongAugment achieves consistent results on external datasets and clinical validation cases, even when the current state-of-the-art methods achieve no better than random performance. The results of this study indicate that without strong augmentation, neural networks are not likely to generalise to variation encountered in clinical practice.

Our study provides a baseline for evaluating and training neural networks intended for clinical practice. Strong augmentation allows networks to perform consistently despite real-world variability, and shifted evaluation can be used to demonstrate this consistency. Although we establish the effectiveness of these methods in medical imaging, both methods are applicable to any domain.

ACKNOWLEDGEMENTS

This work was supported by Cancer Foundation Finland [304667, 191118], Jane and Aatos Erkko Foundation [290520], Academy of Finland [322675] and Hospital District of Helsinki and Uusimaa [TYH2018214, TYH2018222, TYH2019235, TYH2019249]. The authors also wish to acknowledge Harry Nisen and Petrus Järvinen for Helsinki RCC database management, FIMM Digital Microscopy and Molecular Pathology Unit supported by HiLIFE and Biocenter Finland for imaging services, and CSC – IT Center for Science, Finland for generous computational resources.

ETHICS STATEMENT

Ethical approvals for the use of human tissue material and clinicopathologic data were obtained from Institutional Ethics Committee of Hospital District of Helsinki and Uusimaa (§70/16.5.2018; HUS/419/2018) and by the National Supervisory Authority for Welfare and Health (VALVIRA, D:no V/38176/2018). According to the national and European Union legislation on noninterventional medical research, the study was conducted without informed individual patient consents by permission of the Hospital District of Helsinki and Uusimaa (§105/21.12.2018; HUS/419/2018). The experiments conformed to the principles set out in the WMA Declaration of Helsinki and the Department of Health and Human Services Belmont Report.

DECLARATION OF COMPETING INTERESTS

The authors have no interests to declare.

CREDIT AUTHORSHIP CONTRIBUTION STATEMENT

Joona Pohjonen: Conceptualisation; Formal analysis; Visualisation; Software; Methodology; Data curation; Roles/Writing - original draft **Carolyn Stürenberg:** Data curation, Writing - review & editing; **Atte Föhr:** Data curation, Formal analysis; **Reija Randen-Brady:** Data curation; **Lassi Luomala:** Data curation; **Jouni Lohi:** Data curation; **Esa Pitkänen:** Funding

acquisition; Resources; Supervision; Writing - review & editing; **Antti Rannikko:** Funding acquisition; Resources; Supervision; Writing - review & editing; **Tuomas Mirtti:** Conceptualisation; Data curation; Funding acquisition; Resources; Supervision; Writing - review & editing;

REFERENCES

- [1] Manuel Salto-Tellez, Perry Maxwell, and Peter Hamilton. Artificial intelligence-the third revolution in pathology. *Histopathology*, 74(3):372–376, 2019.
- [2] Xiaoxuan Liu, Livia Faes, Aditya U Kale, Siegfried K Wagner, Dun Jack Fu, Alice Bruynseels, Thushika Mahendiran, Gabriella Moraes, Mohith Shamdass, Christoph Kern, et al. A comparison of deep learning performance against health-care professionals in detecting diseases from medical imaging: a systematic review and meta-analysis. *The lancet digital health*, 1(6):e271–e297, 2019.
- [3] Eric J Topol. High-performance medicine: the convergence of human and artificial intelligence. *Nature medicine*, 25(1):44–56, 2019.
- [4] Gabriele Campanella, Matthew G Hanna, Luke Geneslaw, Allen Mirafior, Vitor Werneck Krauss Silva, Klaus J Busam, Edi Brogi, Victor E Reuter, David S Klimstra, and Thomas J Fuchs. Clinical-grade computational pathology using weakly supervised deep learning on whole slide images. *Nature medicine*, 25(8):1301–1309, 2019.
- [5] Kunal Nagpal, Davis Foote, Yun Liu, Po-Hsuan Cameron Chen, Ellery Wulczyn, Fraser Tan, Niels Olson, Jenny L Smith, Arash Mohtashamian, James H Wren, et al. Development and validation of a deep learning algorithm for improving gleason scoring of prostate cancer. *NPJ digital medicine*, 2(1):1–10, 2019.
- [6] Thomas de Bel, Meyke Hermsen, Jesper Kers, Jeroen van der Laak, and Geert Litjens. Stain-transforming cycle-consistent generative adversarial networks for improved segmentation of renal histopathology. In *International Conference on Medical Imaging with Deep Learning—Full Paper Track*, 2018.
- [7] Yun Liu, Timo Kohlberger, Mohammad Norouzi, George E Dahl, Jenny L Smith, Arash Mohtashamian, Niels Olson, Lily H Peng, Jason D Hipp, and Martin C Stumpe. Artificial intelligence-based breast cancer nodal metastasis detection: Insights into the black box for pathologists. *Archives of pathology & laboratory medicine*, 143(7):859–868, 2019.
- [8] John R Zech, Marcus A Badgeley, Manway Liu, Anthony B Costa, Joseph J Titano, and Eric Karl Oermann. Variable generalization performance of a deep learning model to detect pneumonia in chest radiographs: a cross-sectional study. *PLoS medicine*, 15(11):e1002683, 2018.
- [9] Julia K Winkler, Christine Fink, Ferdinand Toberer, Alexander Enk, Teresa Deinlein, Rainer Hofmann-Wellenhof, Luc Thomas, Aimilios Lallas, Andreas Blum, Wilhelm Stolz, et al. Association between surgical skin markings in dermoscopic images and diagnostic performance of a deep learning convolutional neural network for

- melanoma recognition. *JAMA dermatology*, 155(10):1135–1141, 2019.
- [10] Alex J DeGrave, Joseph D Janizek, and Su-In Lee. Ai for radiographic covid-19 detection selects shortcuts over signal. *Nature Machine Intelligence*, pages 1–10, 2021.
- [11] Jeroen van der Laak, Geert Litjens, and Francesco Ciompi. Deep learning in histopathology: the path to the clinic. *Nature medicine*, 27(5):775–784, 2021.
- [12] Joona Pohjonen, Carolin Stürenberg, Antti Rannikko, Tuomas Mirtti, and Esa Pitkänen. Spectral decoupling for training transferable neural networks in medical imaging. *iScience*, page 103767, 2022.
- [13] Myura Nagendran, Yang Chen, Christopher A Lovejoy, Anthony C Gordon, Matthieu Komorowski, Hugh Harvey, Eric J Topol, John PA Ioannidis, Gary S Collins, and Mahiben Maruthappu. Artificial intelligence versus clinicians: systematic review of design, reporting standards, and claims of deep learning studies. *Bmj*, 368, 2020.
- [14] Yaniv Ovadia, Emily Fertig, Jie Ren, Zachary Nado, David Sculley, Sebastian Nowozin, Joshua Dillon, Balaji Lakshminarayanan, and Jasper Snoek. Can you trust your model’s uncertainty? evaluating predictive uncertainty under dataset shift. *Advances in neural information processing systems*, 32, 2019.
- [15] Digital compression and coding of continuous-tone still images: Requirements and guidelines, 2 1992.
- [16] Birgid Schömig-Markiefka, Alexey Prylukhin, Wolfgang Hulla, Andrey Bychkov, Junya Fukuoka, Anant Madabhushi, Viktor Achter, Lech Nieroda, Reinhard Büttner, Alexander Quaas, et al. Quality control stress test for deep learning-based diagnostic model in digital pathology. *Modern Pathology*, 34(12):2098–2108, 2021.
- [17] Yijiang Chen, Andrew Janowczyk, and Anant Madabhushi. Quantitative assessment of the effects of compression on deep learning in digital pathology image analysis. *JCO clinical cancer informatics*, 4:221–233, 2020.
- [18] Timo Kohlberger, Yun Liu, Melissa Moran, Po-Hsuan Cameron Chen, Trissia Brown, Jason D Hipp, Craig H Mermel, and Martin C Stumpe. Whole-slide image focus quality: Automatic assessment and impact on ai cancer detection. *Journal of pathology informatics*, 10(1):39, 2019.
- [19] Gaël Varoquaux and Veronika Cheplygina. Machine learning for medical imaging: methodological failures and recommendations for the future. *npj Digital Medicine*, 5(1):1–8, 2022.
- [20] Robert Geirhos, Jörn-Henrik Jacobsen, Claudio Michaelis, Richard Zemel, Wieland Brendel, Matthias Bethge, and Felix A Wichmann. Shortcut learning in deep neural networks. *Nature Machine Intelligence*, 2(11):665–673, 2020.
- [21] Marc Macenko, Marc Niethammer, J. S. Marron, David Borland, John T. Woosley, Xiaojun Guan, Charles Schmitt, and Nancy E. Thomas. A method for normalizing histology slides for quantitative analysis. pages 1107–1110, 2009.
- [22] Andrew Janowczyk, Ajay Basavanahally, and Anant Madabhushi. Stain normalization using sparse autoencoders (stanosa): application to digital pathology. *Computerized Medical Imaging and Graphics*, 57:50–61, 2017.
- [23] Hyungjoo Cho, Sungbin Lim, Gunho Choi, and Hyunseok Min. Neural stain-style transfer learning using gan for histopathological images. *arXiv preprint arXiv:1710.08543*, 2017.
- [24] Yushan Zheng, Zhiguo Jiang, Haopeng Zhang, Fengying Xie, Dingyi Hu, Shujiao Sun, Jun Shi, and Chenghai Xue. Stain standardization capsule for application-driven histopathological image normalization. *IEEE journal of biomedical and health informatics*, 25(2):337–347, 2020.
- [25] David Tellez, Geert Litjens, Péter Bándi, Wouter Bulten, John-Melle Bokhorst, Francesco Ciompi, and Jeroen van der Laak. Quantifying the effects of data augmentation and stain color normalization in convolutional neural networks for computational pathology. *Medical image analysis*, 58:101544, 2019.
- [26] Nicola Michielli, Alessandro Caputo, Manuela Scotto, Alessandro Mogetta, Orazio Antonino Maria Pennisi, Filippo Molinari, Davide Balmativola, Martino Bosco, Alessandro Gambella, Jasna Metovic, et al. Stain normalization in digital pathology: Clinical multi-center evaluation of image quality. *Journal of Pathology Informatics*, page 100145, 2022.
- [27] Mohammad Pezeshki, Oumar Kaba, Yoshua Bengio, Aaron C Courville, Doina Precup, and Guillaume Lajoie. Gradient starvation: A learning proclivity in neural networks. *Advances in Neural Information Processing Systems*, 34, 2021.
- [28] David Tellez, Maschenka Balkenhol, Irene Otte-Höller, Rob van de Loo, Rob Vogels, Peter Bult, Carla Wauters, Willem Vreuls, Suzanne Mol, Nico Karssemeijer, Geert Litjens, Jeroen van der Laak, and Francesco Ciompi. Whole-slide mitosis detection in h amp;e breast histology using phh3 as a reference to train distilled stain-invariant convolutional networks. *IEEE Transactions on Medical Imaging*, 37(9):2126–2136, 2018.
- [29] Ekin D Cubuk, Barret Zoph, Dandelion Mane, Vijay Vasudevan, and Quoc V Le. Autoaugment: Learning augmentation strategies from data. In *Proceedings of the IEEE/CVF Conference on Computer Vision and Pattern Recognition*, pages 113–123, 2019.
- [30] Ekin D Cubuk, Barret Zoph, Jonathon Shlens, and Quoc V Le. Randaugment: Practical automated data augmentation with a reduced search space. In *Proceedings of the IEEE/CVF Conference on Computer Vision and Pattern Recognition Workshops*, pages 702–703, 2020.
- [31] Samuel G Müller and Frank Hutter. Trivialaugment: Tuning-free yet state-of-the-art data augmentation. In *Proceedings of the IEEE/CVF International Conference on Computer Vision*, pages 774–782, 2021.
- [32] Irwan Bello, William Fedus, Xianzhi Du, Ekin Dogus Cubuk, Aravind Srinivas, Tsung-Yi Lin, Jonathon Shlens, and Barret Zoph. Revisiting resnets: Improved training and scaling strategies. *Advances in Neural Information Processing Systems*, 34, 2021.
- [33] Alexander Buslaev, Vladimir I Iglovikov, Eugene Khvedchenya, Alex Parinov, Mikhail Druzhinin, and Alexandr A

- Kalinin. Alumentations: fast and flexible image augmentations. *Information*, 11(2):125, 2020.
- [34] Sébastien Marcel and Yann Rodriguez. Torchvision the machine-vision package of torch. In *Proceedings of the 18th ACM international conference on Multimedia*, pages 1485–1488, 2010.
- [35] Khrystyna Faryna, Jeroen van der Laak, and Geert Litjens. Tailoring automated data augmentation to h&e-stained histopathology. In *Medical Imaging with Deep Learning*, 2021.
- [36] Tom Ching LingChen, Ava Khonsari, Amirreza Lashkari, Mina Rafi Nazari, Jaspreet Singh Sambee, and Mario A Nascimento. Uniformaugment: A search-free probabilistic data augmentation approach. *arXiv preprint arXiv:2003.14348*, 2020.
- [37] Nitish Srivastava, Geoffrey Hinton, Alex Krizhevsky, Ilya Sutskever, and Ruslan Salakhutdinov. Dropout: a simple way to prevent neural networks from overfitting. *The journal of machine learning research*, 15(1):1929–1958, 2014.
- [38] Gao Huang, Yu Sun, Zhuang Liu, Daniel Sedra, and Kilian Q Weinberger. Deep networks with stochastic depth. In *European conference on computer vision*, pages 646–661. Springer, 2016.
- [39] Hongyi Zhang, Moustapha Cisse, Yann N Dauphin, and David Lopez-Paz. mixup: Beyond empirical risk minimization. *arXiv preprint arXiv:1710.09412*, 2017.
- [40] Sangdoo Yun, Dongyoon Han, Seong Joon Oh, Sanghyuk Chun, Junsuk Choe, and Youngjoon Yoo. Cutmix: Regularization strategy to train strong classifiers with localizable features. In *Proceedings of the IEEE/CVF international conference on computer vision*, pages 6023–6032, 2019.
- [41] Jungmin Kwon, Jeongseop Kim, Hyunseo Park, and In Kwon Choi. Asam: Adaptive sharpness-aware minimization for scale-invariant learning of deep neural networks. In *International Conference on Machine Learning*, pages 5905–5914. PMLR, 2021.
- [42] Diederik P Kingma and Jimmy Ba. Adam: A method for stochastic optimization. *arXiv preprint arXiv:1412.6980*, 2014.
- [43] Christian Szegedy, Vincent Vanhoucke, Sergey Ioffe, Jon Shlens, and Zbigniew Wojna. Rethinking the inception architecture for computer vision. In *Proceedings of the IEEE conference on computer vision and pattern recognition*, pages 2818–2826, 2016.
- [44] Adam Paszke, Sam Gross, Francisco Massa, Adam Lerer, James Bradbury, Gregory Chanan, Trevor Killeen, Zeming Lin, Natalia Gimelshein, Luca Antiga, Alban Desmaison, Andreas Kopf, Edward Yang, Zachary DeVito, Martin Raison, Alykhan Tejani, Sasank Chilamkurthy, Benoit Steiner, Lu Fang, Junjie Bai, and Soumith Chintala. Pytorch: An imperative style, high-performance deep learning library. In H. Wallach, H. Larochelle, A. Beygelzimer, F. d’Alché-Buc, E. Fox, and R. Garnett, editors, *Advances in Neural Information Processing Systems 32*, pages 8024–8035. Curran Associates, Inc., 2019.
- [45] Ross Wightman. Pytorch image models. <https://github.com/rwightman/pytorch-image-models>, 2019.
- [46] Wouter Bulten, Kimmo Kartasalo, Po-Hsuan Cameron Chen, Peter Ström, Hans Pinckaers, Kunal Nagpal, Yuan-nan Cai, David F Steiner, Hester van Boven, Robert Vink, et al. Artificial intelligence for diagnosis and gleason grading of prostate cancer: the panda challenge. *Nature medicine*, pages 1–10, 2022.
- [47] Wouter Bulten, Péter Bándi, Jeffrey Hoven, Rob van de Loo, Johannes Lotz, Nick Weiss, Jeroen van der Laak, Bram van Ginneken, Christina Hulsbergen-van de Kaa, and Geert Litjens. Peso: Prostate epithelium segmentation on h&e-stained prostatectomy whole slide images, 2018. Accessed: 05.03.2021.
- [48] Jonathan I Epstein, Lars Egevad, Mahul B Amin, Brett Delahunt, John R Srigley, and Peter A Humphrey. The 2014 international society of urological pathology (isup) consensus conference on gleason grading of prostatic carcinoma. *The American journal of surgical pathology*, 40(2):244–252, 2016.
- [49] Davood Karimi, Guy Nir, Ladan Fazli, Peter C Black, Larry Goldenberg, and Septimiu E Salcudean. Deep learning-based gleason grading of prostate cancer from histopathology images—role of multiscale decision aggregation and data augmentation. *IEEE journal of biomedical and health informatics*, 24(5):1413–1426, 2019.
- [50] Joona Pohjonen and Valeria Ariotta. Histoprep: Preprocessing large medical images for machine learning made easy! <https://github.com/jopo666/HistoPrep>, 2021.
- [51] David H Wolpert and William G Macready. No free lunch theorems for optimization. *IEEE transactions on evolutionary computation*, 1(1):67–82, 1997.
- [52] Olga Russakovsky, Jia Deng, Hao Su, Jonathan Krause, Sanjeev Satheesh, Sean Ma, Zhiheng Huang, Andrej Karpathy, Aditya Khosla, Michael Bernstein, Alexander C. Berg, and Li Fei-Fei. ImageNet Large Scale Visual Recognition Challenge. *International Journal of Computer Vision (IJCV)*, 115(3):211–252, 2015.

SUPPLEMENTARY FIGURES

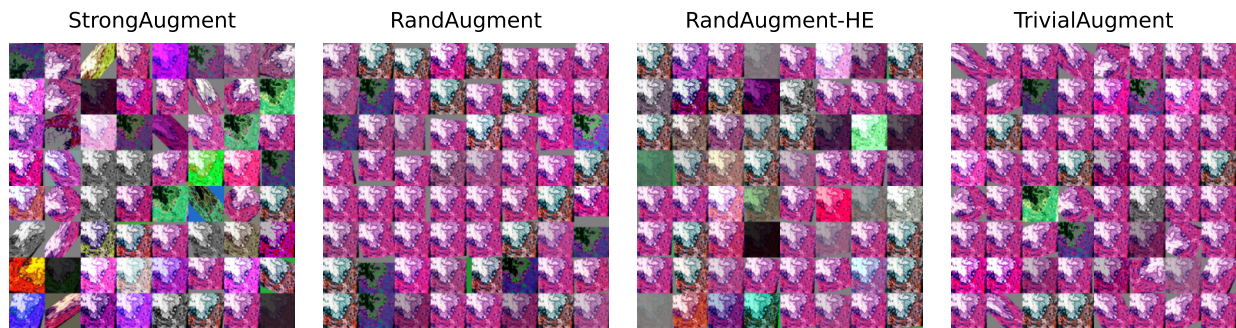


Figure S1: Examples of augmented images using StrongAugment with $p = 0.4$, RandAugment with $m = 10$ and $n = 2$, RandAugment-HE with $m = 5$ and $n = 3$ and TrivialAugment. Images augmented with StrongAugment contain significantly more variability than any of the other methods.

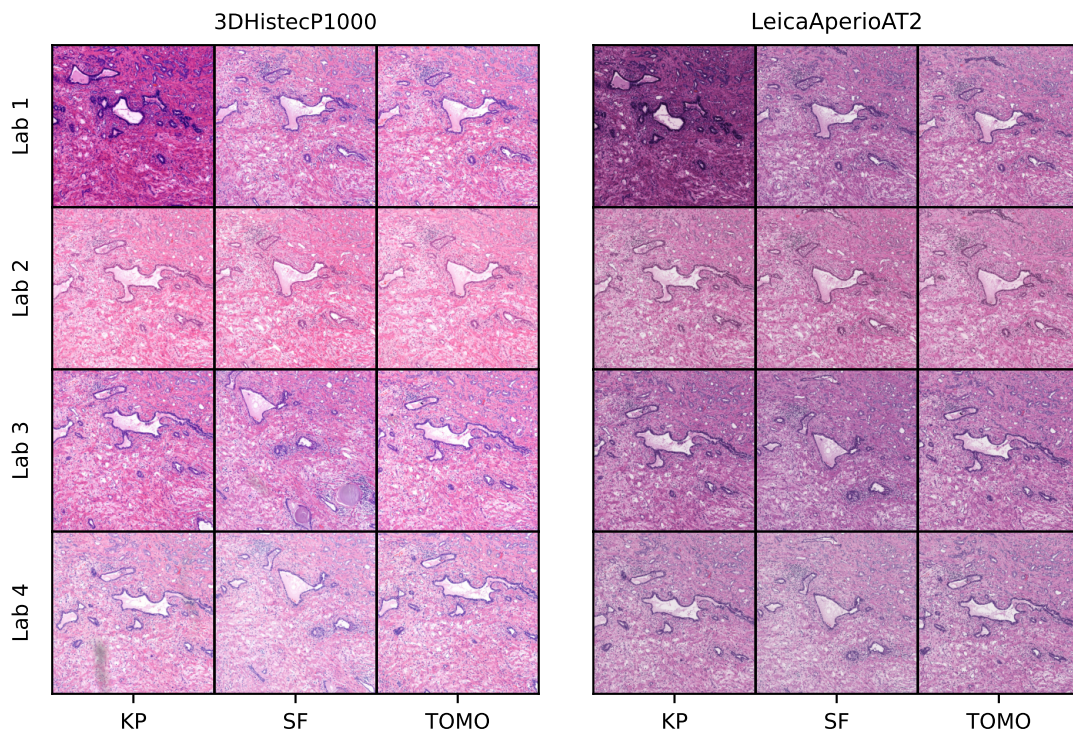


Figure S2: Same region of interest from sample 1 serial sections. There is considerable variation in the scanned images due to variability between medical centres, slide glasses and scanners. Nevertheless, neural networks intended for clinical practice should achieve consistent performance on each clinical validation case.

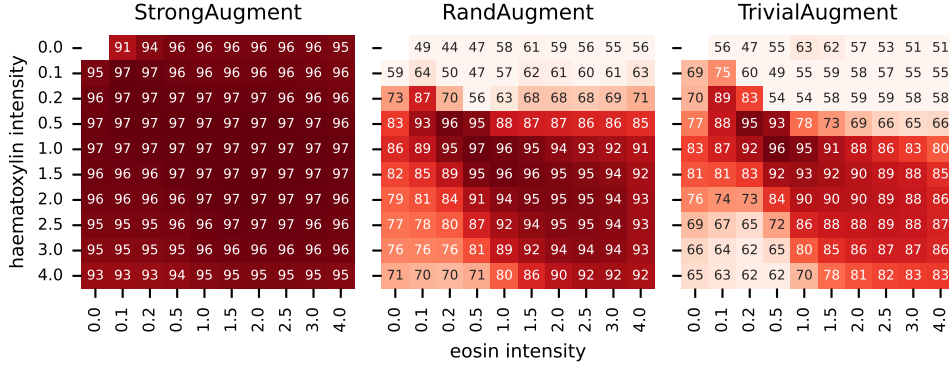


Figure S3: Robustness of neural networks, trained on the Helsinki30 dataset with weight decay instead of spectral decoupling, to distribution shifts caused by differences in the haematoxylin and eosin stain intensities. Each cell represents a given distribution-shifted dataset $stain(X_{PES0}, h, e)$, where h and e denote the magnitudes for haematoxylin and eosin stains, respectively. Cells are annotated with mean AUROC $\times 100$ value for the five trained networks, rounded to the closest integer. Even without spectral decoupling, StrongAugment achieves consistent results for each dataset. Networks trained with RandAugment or TrivialAugment are more dependent on spectral decoupling and achieve up to 25 percentage points lower AUROC than in Figure 5.

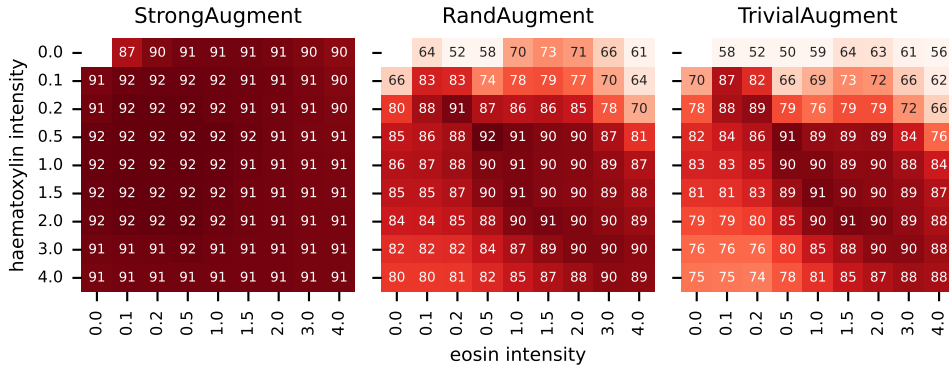


Figure S4: Robustness of neural networks, trained on the HelsinkiRCC dataset with either StrongAugment, RandAugment, or TrivialAugment, to distribution shifts caused by differences in the haematoxylin and eosin stain intensities. Each cell represents a given distribution-shifted dataset $stain(X_{val}, h, e)$, where h and e denote the magnitudes for haematoxylin and eosin stains, respectively, and x_{val} the validation split of HelsinkiRCC dataset. Cells are annotated with mean AUROC $\times 100$ value for the five trained networks, rounded to the closest integer. Neural networks trained with StrongAugment retain performance on all datasets, even when networks trained with RandAugment or TrivialAugment quickly degrade to no better than random discrimination.